Journal of the Less-Common Metals, 108 (1985) 89 - 105

ALLOYING BEHAVIOUR OF MANGANESE WITH BASIC METALS: Pr–Mn SYSTEM

A. SACCONE, S. DELFINO and R. FERRO

Istituto di Chimica Generale dell'Università, Università di Genova, viale Benedetto XV, 3, Genoa (Italy)

(Received August 3, 1984)

Summary

The general properties of rare earth–manganese alloys are described and reviewed. The Pr–Mn system was studied using differential thermal analysis, X-ray examination, metallography and microprobe analysis. Both the stable phase diagram and information on the metastable equilibria were obtained. Evidence of the peritectic formation (790 °C) of Pr_6Mn_{23} (Th_6Mn_{23}-type structure) and the decomposition (about 650 °C) of the same phase appears in the stable diagram. A eutectic (660 °C, 25 at.% Mn) was also observed. The peritectic formation (740 °C) of $PrMn_2$ (hexagonal Laves phase) took place under metastable conditions. The various methods of preparing these alloys are discussed and their strong reactivity with alumina is studied. Finally it is shown that the Pr–Mn diagram fits well in the sequence of the known diagrams of manganese with the rare earths and the basic metals. The relation between the ratio of the atomic dimensions, the valence electron number and the mutual reactivity is emphasized.

1. Introduction

Manganese is known to be generally very reactive with other elements; its binary state diagrams often show very complicated sequences of intermediate phases. However, this reactivity decreases steadily towards the most basic metals at the extreme left of the periodic table. Manganese shows a different pattern of behaviour with these metals: in these cases we observe not only complete insolubility in the solid state and the absence of intermediate phases, but also relatively wide miscibility gaps in the liquid state (see for instance the data summarized in ref. 1). The reactivity of manganese with the rare earths (R) is located at the boundary between the two types of alloying behaviour discussed above and is therefore particularly significant. The study of the rare earth alloys is also very interesting from a more general point of view. When a metal is alloyed with the various rare earth elements, a systematic variation in the properties is observed; this can be used to evaluate the effects of the characteristics of the components on those of their

0022-5088/85/$3.30

alloys and compounds (the shapes of the phase diagrams, the number and type of intermediate phases etc.) (see, for instance, the reports of investigations of the systematics of the rare earth alloys with metals such as lead [2], silver [3], gallium [4] and indium [5] and the critical review by Gschneidner and Calderwood [6]).

2. General comments on R–Mn alloys

The behaviour of divalent rare earths (europium and ytterbium) [7] with the R–Mn alloy group is well established and is similar to that of metals such as calcium and barium (no intermediate compounds, almost complete solid state immiscibility and a large miscibility gap in the liquid state). However, the behaviour changes steadily in the trivalent rare earth sequence on proceeding from the light elements (lanthanum [8] and cerium [9 - 11] which in this case behave like divalent rare earths) towards the heavy elements. The two types of phase diagrams are represented in Fig. 1. The La–Mn diagram [8] is shown in Fig. 1(a) and the Er–Mn diagram [12] in Fig. 1(b).

The diagrams reported in the literature for Tb–Mn [13], Dy–Mn [12], Ho–Mn [12] and Gd–Mn [12] are very similar to that of Er–Mn. All these

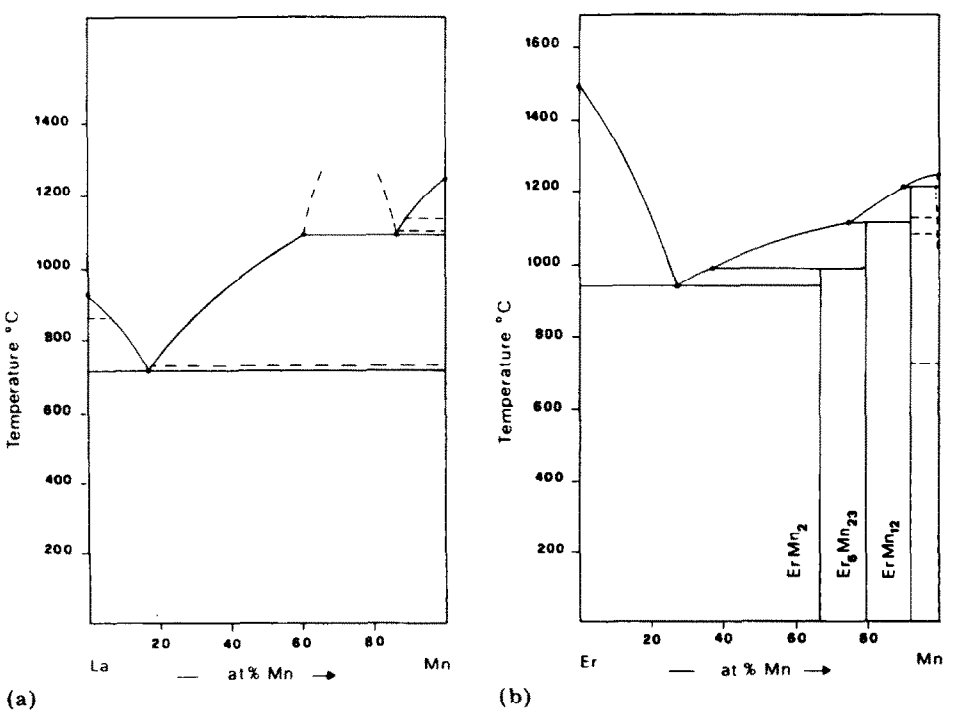

Fig. 1. Examples of phase diagrams of manganese with light and heavy rare earths: (a) La–Mn system [8]; (b) Er–Mn system [12].

systems show peritectically melting phases RMn_2, R_6Mn_{23} and RMn_{12}. Only Nd_6Mn_{23} and $NdMn_{12}$ have been included in the phase diagram for the Mn–Nd system although another phase ($NdMn_2$) has been reported by Tesljuk *et al.* [14]. The only positively identified phase in the Sm–Mn phase diagram [13] is Sm_6Mn_{23}; however, $SmMn_2$ [15] and $SmMn_{12}$ [16] phases have been reported in the literature.

Various techniques have been used and described for the preparation of the various phases in the R–Mn systems and their crystal structures have been studied. The RMn_2 compounds have been described as Laves phases of both the cubic *cF*24 ($MgCu_2$) type (for R ≡ Sm [15], Gd [17 - 19], Tb [17], Dy [17 - 19], Ho [17, 19], Er [15]) and the hexagonal *hP*12 ($MgZn_2$) type (for R ≡ Pr [14], Nd [14], Sm [15], Ho [19], Er [14, 19, 20], Tm [14, 20], Lu [14]). The R_6Mn_{23} compounds (for which other stoichiometries such as RMn_4 and RMn_5 have been proposed in the past) have been described as belonging to the cubic *cF*116 (Th_6Mn_{23}) type [16, 19, 21]. The RMn_{12} compounds are tetragonal *tI*26 ($ThMn_{12}$) type [19, 22].

The phase diagram of the Pr–Mn system, which should have a shape intermediate between those of the La–Mn and Ce–Mn systems and those of subsequent R–Mn systems, is unknown. Moreover the data available in the literature are contradictory so that an investigation of this system seemed appropriate. A number of experimental difficulties were encountered during this investigation, in agreement with indications given in the literature. Effects due to changes in the thermal treatment (variations in the heating or cooling rates, small variations of annealing temperatures or times etc.) were encountered. Marked effects were also produced by impurities in the specimens and by contamination resulting from reactions with crucible components.

3. Literature data for Pr–Mn phases

As stated above no information regarding the phase diagram of the Pr–Mn system is available.

Tesljuk *et al.* [15] investigated $PrMn_2$ alloys during studies of alloys of manganese with neodymium, samarium, erbium, thulium, lutetium and praseodymium. The alloys were prepared by fusing electrolytic manganese with the rare earth metals in corundum crucibles in a Tamman furnace (helium atmosphere) followed by slow cooling. Tesljuk *et al.* found compounds with the hexagonal $MgZn_2$-type structure in all except the samarium alloys, and they identified $PrMn_2$ with a = 5.61 Å and c = 9.16 Å (c/a = 1.63). The praseodymium and neodymium alloys contained β-Mn in addition to RMn_2.

Kripyakevich *et al.* [23] observed phases with the cubic Th_6Mn_{23}-type structure during a study of alloys with the 6:23 stoichiometry; they reported a = 12.75 Å for the cubic cell. These researchers prepared the alloys by compacting mixtures of the rare earth and manganese in the stoichiometric ratio corresponding to R_6Mn_{23}. The compacts were sealed in quartz tubes under

an argon atmosphere. They were wrapped in molybdenum foil in order to avoid any contact with the quartz walls and were sintered at 700 - 900 °C for 100 - 240 h.

Oesterreicher and coworkers investigated the structural and high temperature magnetic properties of the pseudobinary systems $PrMn_2$–$ErMn_2$ [24], $PrMn_2$–$GdMn_2$ [25] and $PrMn_2$–$TbMn_2$ [25] and ruled out the existence of the hexagonal $MgZn_2$-type phase; they suggested the existence of a b.c.c. phase of the α-Mn type (χ phase) with a = 8.902 Å at 950 K and a phase of approximate composition $PrMn_2$ with a Th_6Mn_{23}-type structure (G phase) with a = 12.690 Å at 1000 K for stoichiometries close to $PrMn_2$. The compounds were formed by induction melting. Pieces of metal were fused together in high purity MgO crucibles under a low pressure argon atmosphere. The samples were subsequently annealed in evacuated Vycor tubes for approximately 200 h at 900 K.

4. Experimental details

The experimental techniques used to prepare and examine the alloys employed in this work are described below.

The praseodymium (nominal purity, 99.9 wt.%) was obtained from Koch-Light Laboratories Ltd. (Gt. Britain), and the manganese (nominal purity, 99.9 wt.%) was in the form of platelets (the lattice constant a of the α-Mn determined using a Debye–Scherrer camera was 8.912 Å compared with the literature value of 8.9139 Å [15]). The alloys (about 1 - 2 g of each) were prepared in an induction furnace; pieces of the constituent metals were fused in small tantalum or molybdenum crucibles which were sealed by welding.

Systematic investigations were performed in view of reports in the literature regarding the preparation of alloys in Al_2O_3 and the possible effects of this material on their structure and characteristics. (The results obtained for alloys prepared in Al_2O_3 will be briefly described although, owing to the heavy contamination, they do not apply to the binary Pr–Mn system.)

The alloys were generally obtained as well-melted ingots which were often brittle, particularly at high manganese contents. The samples were examined both in the as-cast condition and after the various heat treatments on samples enclosed in tantalum crucibles described below. Differential thermal analysis, metallographic analysis, electron probe microanalysis and X-ray diffraction analysis (powder method) were used to characterize the alloys.

The heating and cooling rates for differential thermal analysis were generally between 8 and 10 °C min^{-1}.

The specimens for microscope and microprobe examination were prepared using SiC papers and diamond polishing; the samples were etched in dilute alcoholic HNO_3 solution to reveal the various phases. Several

samples were examined under a scanning electron microscope and in a few cases a quantitative electron probe microanalysis of the phases was also carried out; quantitative elemental analysis was performed using an energy dispersive X-ray analyser. The intensities, corrected for atomic number, absorption and fluorescence effects, were compared with those of standards.

The X-ray examination was carried out on powder samples using the Debye method with Fe Kα radiation; the experimental crystallographic constants were refined using a least-squares interpolation and d was corrected by applying the Nelson–Riley function. In most cases the observed diffraction intensities were compared with the calculated values obtained by means of a program written for the Hewlett-Packard HP 9825T computer.

Results

Table 1 summarizes the results of X-ray analysis and of optical and electron microscopy associated with microprobe analysis for groups of specimens which had been subjected to various thermal treatments. Figure 2 shows the equilibrium diagram proposed on the basis of our observations, and Fig. 3 represents a metastable portion of the same system.

5.1. Phase diagram

The following comments may be useful for a better understanding of the reported data.

5.1.1. Terminal solubilities

On the basis of differential thermal analysis and by analogy with the Ce–Mn system studied by Thamer [11] we propose for the praseodymium-rich alloys an inverse peritectic reaction (at a temperature very close to the estimated eutectic temperature of 665 °C). The addition of manganese lowers the $\alpha \rightleftarrows \beta$ transformation temperature to this value. The solubilities in β-Pr and α-Pr at this temperature are estimated to be 6 at.% Mn and 1 - 2 at.% Mn respectively.

The $\gamma \rightleftarrows \delta$ and $\beta \rightleftarrows \gamma$ transformations in the other terminal area of the system (manganese-rich alloys) seem to be unaffected by praseodymium additions. The $\alpha \rightleftarrows \beta$ transformation has been observed on cooling at temperatures lower than that characteristic of pure manganese. The shape of the thermal effect associated with this transformation is very similar to that observed in pure manganese. The amplitudes of these effects increase on going towards 100 at.% Mn; however, the temperatures themselves show an erratic distribution (sluggishness?) and therefore only a tentative value of 600 °C is reported in the phase diagram. No claims are made for the accuracy of the description of this region of the diagram.

Microprobe analysis suggested that praseodymium was negligibly soluble in manganese.

TABLE 1

Selected Pr–Mn samples

Nominal composition (at.%)	*Thermal treatment*	*Micrographic appearance supported by microprobe analysis*	*Diffraction lines observed in the powder photographs*
35	Melted and cooled at 10 °C min^{-1}	Eutectic (Pr + $PrMn_2$) + $PrMn_2$ + Mn	—
35	Annealed at 730 °C for 150 h (water quenched)	Eutectic (Pr + Pr_6Mn_{23}) + Pr_6Mn_{23} + Mn (small quantities)	—
45	Melted and cooled at 10 °C min^{-1}	Eutectic (Pr + $PrMn_2$) + $PrMn_2$ + Mn	$PrMn_2$ (weak)
45	Annealed at 730 °C for 150 h (water quenched)	Eutectic (Pr + Pr_6Mn_{23}) + Pr_6Mn_{23} + Mn (small quantities)	Pr_6Mn_{23}
66.6	Melted and cooled at 10 °C min^{-1}	Eutectic (Pr + $PrMn_2$) + $PrMn_2$ + Mn	$PrMn_2$ (weak)
66.6	Melted and cooled at 10 °C min^{-1}; annealed at 650 °C for 250 h (water quenched)	Mn + Pr	—
66.6	Annealed at 900 °C for 3 h (water quenched)	Mn + eutectic (very fine particles not microanalysed)	β-Mn
66.6	Annealed at 730 °C for 150 h (water quenched)	Eutectic (Pr + Pr_6Mn_{23}) + Pr_6Mn_{23} + Mn (small quantities)	Pr_6Mn_{23}
66.6	Annealed at 700 °C for 150 h (water quenched)	Eutectic (Pr + Pr_6Mn_{23}) + Pr_6Mn_{23} + Mn (small quantities)	Pr_6Mn_{23}
66.6	Annealed at 700 °C for 150 h + 600 °C for 700 h (water quenched)	Pr + Mn	α-Mn
75	Melted and cooled at 10 °C min^{-1}	Eutectic (Pr + $PrMn_2$) + $PrMn_2$ + Mn	—
75	Annealed at 730 °C for 150 h (water quenched)	Eutectic (Pr + Pr_6Mn_{23}) + Pr_6Mn_{23} + Mn	Pr_6Mn_{23}
75	Annealed at 720 °C for 5 h (in DTA apparatus), cooled to 400 °C at 2 °C min^{-1}	Pr_6Mn_{23} + Mn + Pr + small quantities of eutectic (Pr + Pr_6Mn_{23})	Pr_6Mn_{23} + α-Mn
75	Annealed at 720 °C for 5 h (in DTA apparatus), cooled to 600 °C at 2 °C min^{-1} and annealed at 600 °C for 48 h (water quenched)	Pr_6Mn_{23} + Mn + Pr	—

75	Annealed at 720 °C for 5 h (in DTA apparatus), cooled until 600 °C at 2 °C min^{-1} and annealed at 600 °C for 250 h (water quenched)	Mn + Pr + Pr_6Mn_{23} (small quantities)	α-Mn
79.3	Annealed at 950 °C for 24 h (water quenched)	Mn + eutectic (very fine particles not microanalysed)	β-Mn
79.3	Annealed at 700 °C for 150 h (water quenched)	Eutectic (Pr + Pr_6Mn_{23}) + Pr_6Mn_{23} + Mn	Pr_6Mn_{23} + α-Mn
84	Melted and cooled at 10 °C min^{-1}	Eutectic (Pr + $PrMn_2$) + $PrMn_2$ + Mn	—
84	Annealed at 700 °C for 150 h (water quenched)	Eutectic (Pr + Pr_6Mn_{23}) + Pr_6Mn_{23} + Mn	Pr_6Mn_{23} + α-Mn
84	Annealed at 700 °C for 150 h + 600 °C for 700 h (water quenched)	Pr + Mn	α-Mn
92.3	Annealed at 950 °C for 24 h (water quenched)	Mn + eutectic (very fine particles not analysed)	β-Mn

DTA, differential thermal analysis.

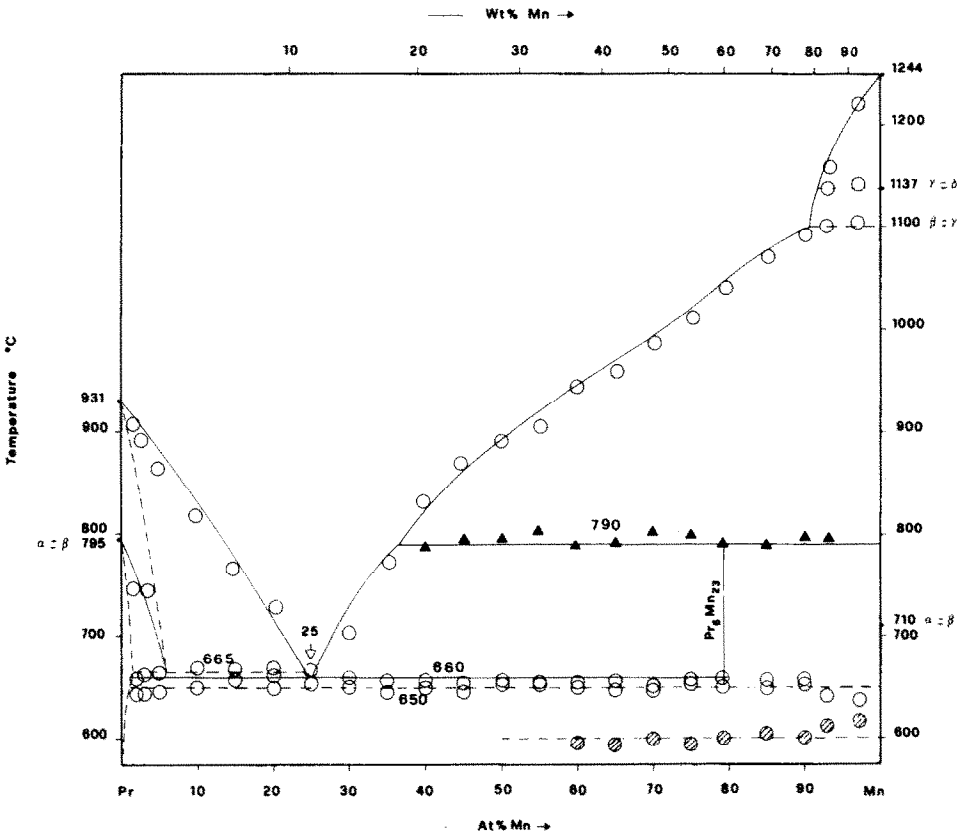

Fig. 2. Phase diagram of the Pr–Mn system: ▲, thermal effects observed mainly on heating; ○, thermal effects observed on both heating and cooling (averaged values); ⊘, thermal effects observed only on cooling (these are believed to be related to a sluggish advancement of the $\alpha \rightleftarrows \beta$ Mn transformation (see text)).

5.1.2. Stable intermetallic compound: Pr_6Mn_{23} phase

The only stable compound existing in the Pr–Mn diagram is Pr_6Mn_{23} which forms peritectically at 790 °C. This compound decomposes upon cooling: at room temperature the only stable phases are pure praseodymium and manganese. It has a cubic *cF*116 (Th_6Mn_{23}) structure which is isostructural with the known R_6Mn_{23} phases and has a lattice parameter *a* of 12.72_5 Å.

As shown in Table 1, in order to prepare this phase the specimens need to be annealed (at temperatures between 700 and 730 °C) for at least a few hours and then quenched. Microprobe analyses performed on more than 20 specimens of this intermediate phase gave manganese contents in the range 78.0 - 79.7 at.% (which is approximately equal to the theoretical value of 79.3 at.% corresponding to the 6:23 stoichiometry). The decomposition can be observed, at least partially, on samples that are cooled to room temperature at about 2 °C min^{-1} (Fig. 4). The decomposition proceeds further

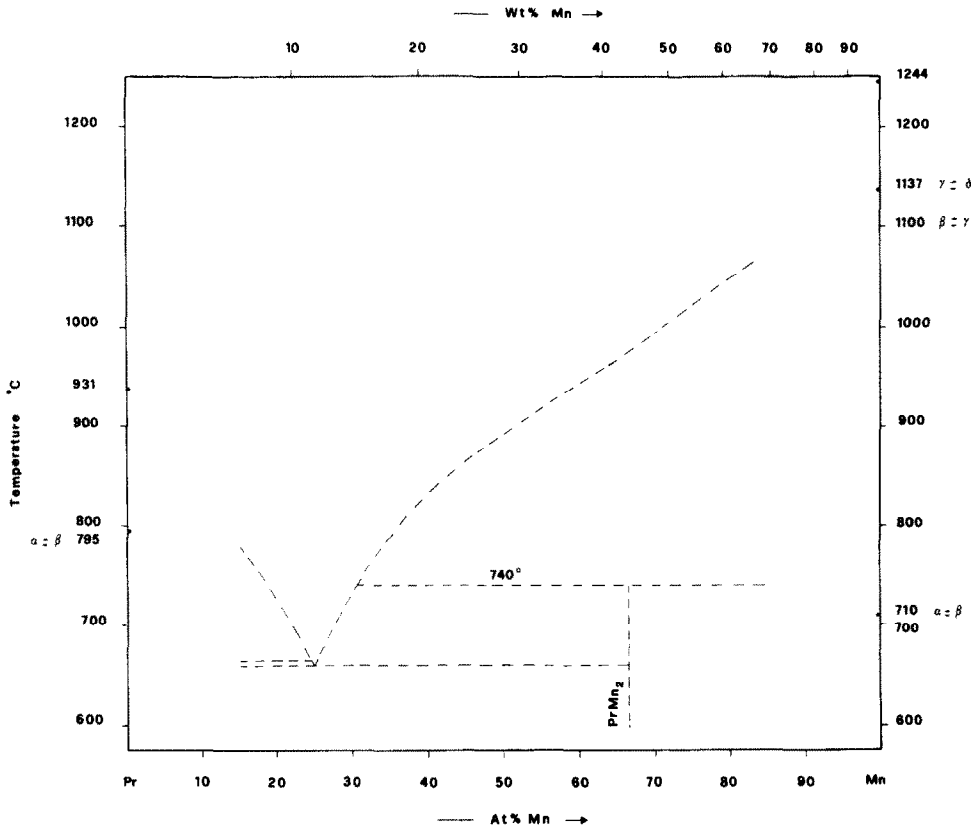

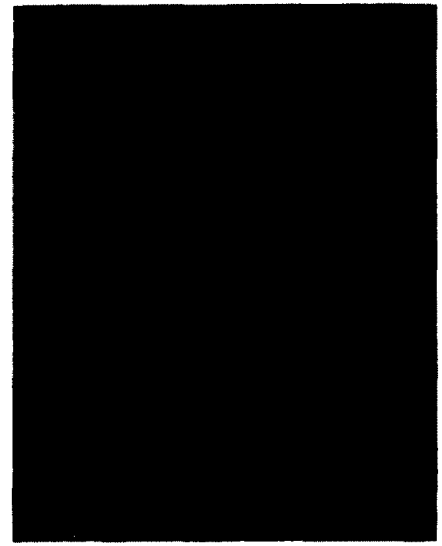

Fig. 3. Peritectic formation of the metastable $PrMn_2$ phase in the Pr–Mn system (only data for alloys containing 35 - 85 at.% Mn are reported).

Fig. 4. Electron micrograph of a Pr–75at.%Mn alloy annealed at 720 °C for 5 h and cooled to 400 °C at 2 °C min^{-1}. The sample was etched in a dilute alcoholic HNO_3 solution. Energy dispersive X-ray analysis revealed the following phases: Pr_6Mn_{23} and eutectic Pr_6Mn_{23} + Pr partially decomposed into manganese and praseodymium. (Magnification, 315x.)

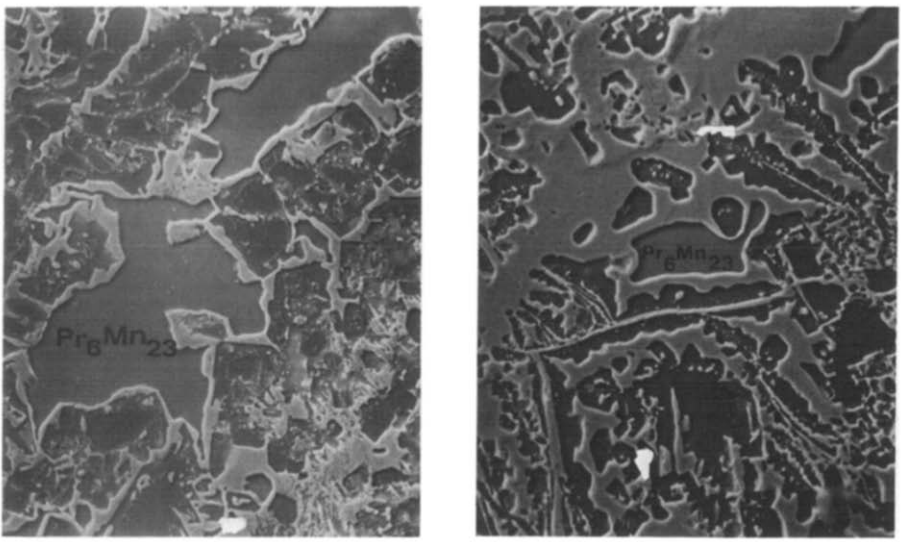

Fig. 5. Electron micrograph of a Pr–75at.%Mn alloy annealed at 720 °C for 5 h, cooled at 2 °C min^{-1}, annealed again at 600 °C for 48 h and finally quenched in water. The sample was etched in a dilute alcoholic HNO_3 solution. The phases are as given in Fig. 4. Comparison with Figs. 4 and 6 reveals almost complete decomposition of the eutectic. (Magnification, 315×.)

Fig. 6. Electron micrograph of a Pr–75at.%Mn alloy annealed at 720 °C for 5 h, cooled to 600 °C at 2 °C min^{-1}, annealed again at 600 °C for 250 h and finally quenched in water. The sample was etched in a dilute alcoholic HNO_3 solution. The phases are as given in Fig. 4. The almost complete disappearance of the Pr_6Mn_{23} phase should be noted. (Magnification, 315×.)

on annealing at 600 °C for example (Figs. 5 - 7). In particular, Fig. 7 shows that the decomposition of Pr_6Mn_{23} results in the formation of the pure elements praseodymium and manganese.

Figure 2 shows the eutectoidal decomposition mechanism proposed for Pr_6Mn_{23} at a temperature of 650 °C (only slightly below the eutectic temperature). The closeness of the two temperatures prevented thermal treatments which would have established whether the above hypothesis of solid state decomposition of the Pr_6Mn_{23} phase was valid. This inconvenience was exacerbated by the presence in the same narrow temperature range of thermal effects connected with the $\alpha \rightleftarrows \beta$ transformations of praseodymium and manganese (the latter transformation is sluggish).

The following values were estimated for the eutectic equilibrium: T = 660 ± 5 °C; composition, 25 ± 1 at.% Mn. Figure 8 shows a photomicrograph of an alloy containing 25 at.% Mn which consists almost entirely of pure eutectic.

5.2. Metastable Pr–Mn equilibria $PrMn_2$ phase

We first note that the formation of intermediate phases was no longer observed in alloys quenched from above 850 °C (see Table 1). In these

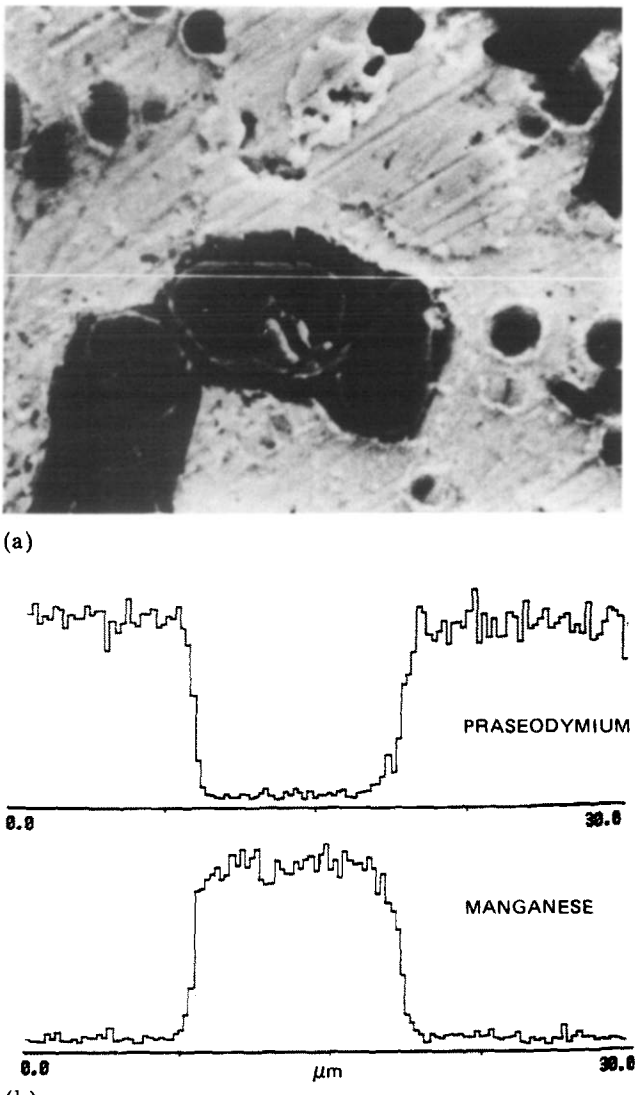

Fig. 7. (a) Electron micrograph and (b) composition profiles of a Pr–66.6at.%Mn alloy annealed at 700 °C for 150 h and at 600 °C for 700 h and finally quenched in water. The composition profiles were taken along the section of the specimen indicated in the electron micrograph by the white line. The praseodymium and manganese contents are given in arbitrary units. It should be noted that the two phases are almost coincident with the pure metals. (Magnification: (a) 1800×.)

cases only primary manganese was observed. The powder photographs show the characteristic diffraction patterns of β-Mn.

The formation of another metastable phase (Laves-type $PrMn_2$) was observed over a large composition range (35 - 85 at.% Mn) when a slow

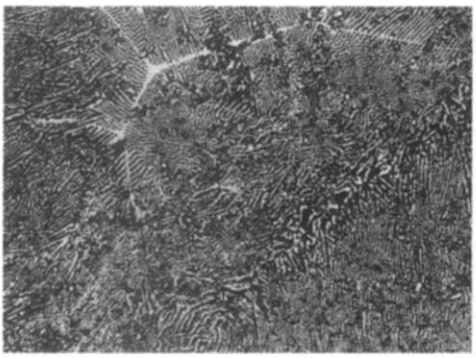

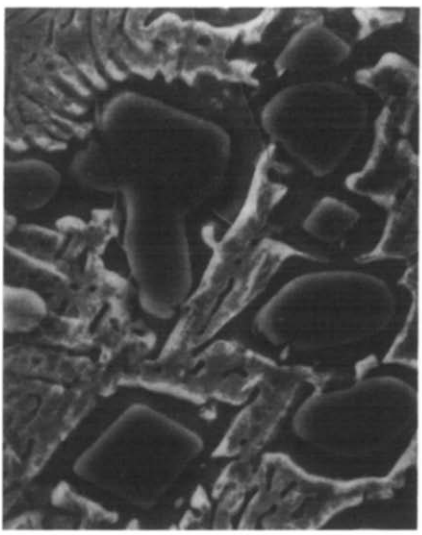

Fig. 8. Micrograph of a Pr–25at.%Mn alloy after differential thermal analysis showing an almost pure eutectic structure. The sample was etched in a dilute alcoholic HNO_3 solution. (Magnification, 147×.)

Fig. 9. Electron micrograph of a Pr–66.6at.%Mn alloy cooled from the melt at 10 °C min^{-1}. The sample was etched in a dilute alcoholic HNO_3 solution. Energy dispersive X-ray analysis revealed the following phases: pure manganese, $PrMn_2$ and eutectic $PrMn_2$ + Pr. The peritectic reaction of manganese to form $PrMn_2$ should be noted. (Magnification, 2016×.)

cooling rate was used. In these samples, however, large quantities of manganese (generally α-Mn) were observed in addition to $PrMn_2$. The peritectic appearance of the $PrMn_2$ phase can be seen in Fig. 9. The composition of this phase has been obtained by microprobe analysis. (In more than 10 specimens the manganese content of the phase was found to be 67 ± 1 at.%). The crystal structure of $PrMn_2$ was confirmed as the hexagonal $hP12$ ($MgZn_2$) type (a = 5.59 Å, c = 9.11 Å and c/a = 1.63) in fair agreement with the literature [14].

The differential thermal analysis of these samples revealed a thermal effect at 740 °C. This effect, which is not observed after annealing for a few hours at temperatures slightly below 740 °C, is ascribed to the metastable peritectic formation of the phase (see Fig. 3). Microprobe and X-ray analyses confirm the disappearance of $PrMn_2$ and the formation of Pr_6Mn_{23} after annealing. Subsequent thermal analysis carried out on heating these samples no longer show the metastable peritectic effect; the stable peritectic is observed instead.

5.3. The reactivity of the Pr–Mn alloys with alumina

Discussions in the literature [24] of the possible stabilizing effect of aluminium on the Pr–Mn phases suggested that a study of the characteristics

of these alloys after melting in sintered alumina crucibles might be interesting. Therefore a number of alloys were kept for a few minutes at the melting temperature in Al_2O_3 crucibles; after cooling the specimens were analysed using the techniques described previously. Aluminium, in addition to praseodymium and manganese, was determined in the various phases using the microprobe. This method of analysis is not very accurate for this element; however, the result obtained, even if semiquantitative, appear to be useful and can be summarized as follows.

5.3.1. Praseodymium (in Al_2O_3)

After the pure liquid metal had been heated in Al_2O_3 at 1000 - 1100 °C for a few minutes aluminium dissolution corresponding to a local composition of 60 - 70 at.% Al was observed. This result agrees with the observations of Pulliam and Fitzsimmons [26] for the reaction between cerium and Al_2O_3 "where both Al and cerium oxide produced appear to be soluble in Ce metal".

5.3.2. Phase with the $MgZn_2$-type structure (in Al_2O_3)

The $PrMn_2$-type phase seems to form much more easily in these conditions (it is probably a stable ternary phase). The estimated aluminium contents of this phase are usually of the order of 5 at.%, in agreement with the data reported by Oesterreicher [24] (the lattice parameters were a = 5.60 Å and c = 9.13 Å).

5.3.3. Th_6Mn_{23}-type phase (in Al_2O_3)

Aluminium does not dissolve to an appreciable extent in the Th_6Mn_{23}-type phase. The Pr_6Mn_{23} compound prepared in Al_2O_3 is a true binary phase.

5.3.4. Phase with the $ThMn_{12}$-type structure (in Al_2O_3)

When manganese-rich alloys are prepared in Al_2O_3 a phase with a structure of the *tI*26 ($ThMn_{12}$) type is obtained (the tetragonal cell parameters were a = 8.91 - 8.96 Å and c = 4.98 - 5.19 Å). An appreciable quantity of aluminium was found in the phase (of the order of 25 - 30 at.%). The crystallographic data can be compared with those reported for the ternary R–Al–Mn alloys. In fact phases with structures that can be considered as variations of the $ThMn_{12}$ type are known to exist in such systems; in particular the RMn_4Al_8 structure (which is a fully ordered $ThMn_{12}$-type derivative) and the RMn_6Al_6 structure (which can be considered as a partially disordered $CeMn_4Al_8$ structure) have been reported [27].

5.3.5. Manganese-type phase (in Al_2O_3)

In contrast with the behaviour of pure manganese which, even when molten, does not react to any appreciable extent with the Al_2O_3 crucible, substantial amounts of aluminium are dissolved in the β-Mn in manganese-rich Pr–Mn alloys. An aluminium content of about 20 - 25 at.% was often observed (see Fig. 10). Even a small quantity of praseodymium seems able

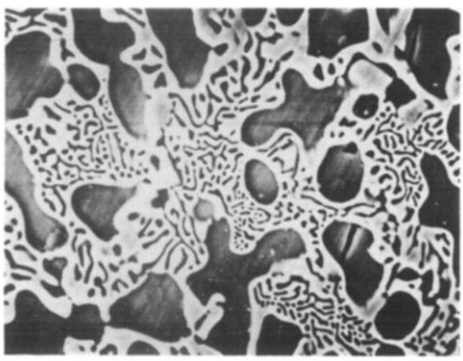

Fig. 10. Electron micrograph of a Pr–84at.%Mn alloy melted in Al_2O_3. The sample was etched in a dilute alcoholic HNO_3 solution. Energy dispersive X-ray analysis revealed the following phases: dark phase, Al–77at.%Mn solid solution; white phase, Pr–Mn–Al compound. This resulted in a $tI26$ ($ThMn_{12}$) type structure. (Magnification, 590×.)

to act as an aluminium carrier. Correspondingly, the lattice constant of β-Mn has approximate values of 6.4 Å compared with the following typical literature values [15]: $a = 6.314_5$ Å (pure manganese), $a = 6.35$ Å (Mn–9at.%Al) and $a = 6.42$ Å (Mn–34at.%Al).

5.3.6. Comments on the reactivity with Al_2O_3

The problems which occur when alloys of this type are melted in Al_2O_3 crucibles are confirmed. Molybdenum crucibles seem to be the most suitable. Tantalum crucibles can also be used; in this case, however, it must be remembered that, particularly for manganese-rich alloys, there is a reaction with the melted manganese which can lead to the formation of $TaMn_2$. Obviously melting by means of a levitation technique could be very useful.

6. General remarks

Figure 11 shows the average atomic volumes of the R–Mn compounds plotted against the atomic number of the rare earth. The values reported for the known R–Mn stoichiometries (RMn_2, R_6Mn_{23} and RMn_{12}) indicate a regular decrease in the average atomic volume with increasing atomic number of the rare earth. In the case of the Pr–Mn system Fig. 11 shows the data for the $PrMn_2$ phase in addition to the data for the Pr_6Mn_{23} phase.

The effect of pressure on these groups of phases (at the boundary between stability and instability) should not be overlooked in discussion of the general properties of these compounds. In particular the investigations of the high pressure synthesis of rare earth dimanganese compounds with the $MgZn_2$ (Laves) structure [28] and the studies of the Yb–Mn system [29] should be noted. The latter system, which exhibits no intermediate phases at ambient pressure, forms the phases Yb_4Mn_3, $YbMn_2$, Yb_6Mn_{23} and Yb_2Mn_{17} at high pressure.

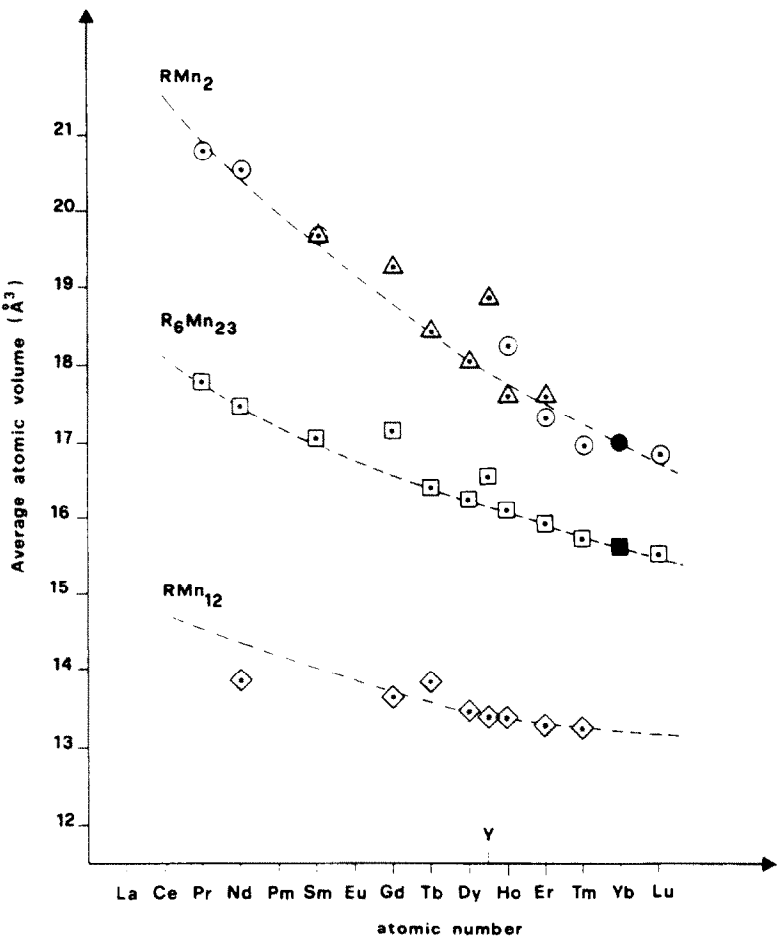

Fig. 11. The average atomic volumes of the RMn_2, R_6Mn_{23} and RMn_{12} compounds *vs.* the atomic number of the rare earth: ⊙, *hP*12 ($MgZn_2$-type) phase; ●, high pressure *hP*12 ($MgZn_2$-type) phase; △, *cF*24 ($MgCu_2$-type) phase; ⊡, *cF*116 (Th_6Mn_{23}-type) phase; ■, high pressure *cF*116 (Th_6Mn_{23}-type) phase; ◇, *tI*26 ($ThMn_{12}$-type) phase. The yttrium data can also be inserted in this graph in a position corresponding to a fictitious atomic number between dysprosium and holmium.

The comments reported above on the characteristics of the various R–Mn phases and on the large effects that several factors (temperature, pressure, cooling rate, annealing time and impurities) have on their stability also seem to be important with respect to possible uses of these substances. Many R–Mn alloys (and their ternary combinations) have been subjected to a systematic study of various properties (*e.g.* magnetic properties) which seem to have promising applications. (Examples of recent work in this area can be found in refs. 30 - 32.) Obviously any reports concerning the method of preparation of the phases and/or their stability or instability may be very useful preliminary information.

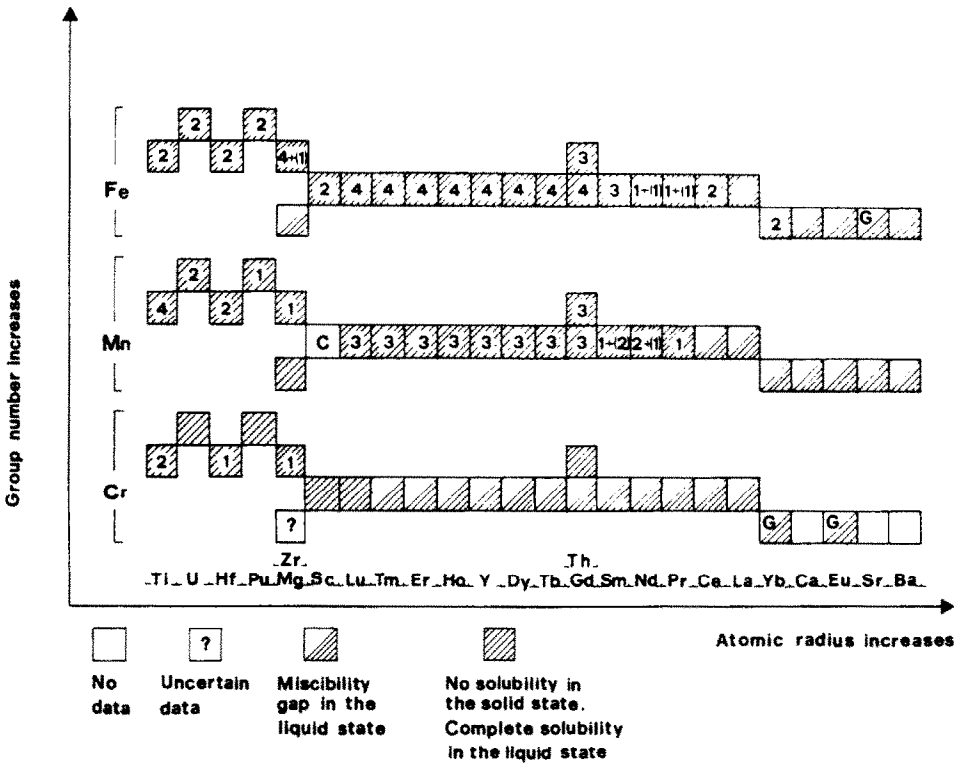

Fig. 12. Alloying behaviour of chromium, manganese and iron with more basic metals. The number of the stable compounds formed is given in each box (C indicates that this number is not well established; G indicates that gas–solid equilibria are involved).

Finally, with respect to the general alloying behaviour of manganese, the Pr–Mn diagram fits well in the sequence of the known diagrams for manganese with the rare earths or, in general, with more basic elements. This general behaviour is summarized in Fig. 12 where it is also compared with the behaviour of iron and chromium (*i.e.* the elements which are adjacent to manganese in the periodic table). The combined effect of the larger atomic dimensions of the basic component and of the lower overall number of valence electrons is clearly related to the decreased mutual reactivity (fewer intermediate phases and lower solubility even in the liquid state).

Acknowledgment

This investigation was carried out within the framework of the scientific research supported by the Italian Consiglio Nazionale delle Ricerche through the "Progetto Finalizzato Metallurgia".

References

1 E. A. Brandes and R. F. Flint, *Manganese Phase Diagrams*, The Manganese Centre, Paris, 1980.
2 K. A. Gschneidner, Jr., and O. D. McMasters, *Monatsh. Chem.*, *102* (1971) 1499.
3 R. Ferro, S. Delfino, R. Capelli and A. Borsese, *J. Less-Common Met.*, *42* (1975) 13.
4 S. P. Yatsenko, A. A. Semyannikov, B. G. Semenov and K. A. Chuntonov, *J. Less-Common Met.*, *64* (1979) 185.
5 S. Delfino, A. Saccone and R. Ferro, *J. Less-Common Met.*, *102* (1984) 289.
6 K. A. Gschneidner, Jr., and F. W. Calderwood, *Critical Evaluation of Binary Rare Earth Phase Diagrams*, Rare-Earth Information Center, Energy and Mineral Resources Research Institute, Iowa State University, Des Moines, IA, to be published.
7 W. G. Moffatt, *The Handbook of Binary Phase Diagrams*, General Electric Company, Schenectady, NY, 1976.
8 L. Rolla and A. Iandelli, *Ber. Dtsch. Chem. Ges.*, *75* (1942) 2091.
9 A. Iandelli, *Atti Accad. Naz. Lincei, Cl. Sci. Fis. Mat. Nat., Rend.*, *13* (1952) 265.
10 M. S. Mirgalovskaia and I. A. Strel'nikova, *Tr. Inst. Metall., Akad. Nauk. S.S.S.R.*, *2* (1957) 135.
11 J. Thamer, *J. Less-Common Met.*, *7* (1964) 341.
12 H. R. Kirchmayr and W. Lugscheider, *Z. Metallkd.*, *58* (1967) 185.
13 H. R. Kirchmayr and W. Lugscheider, *Z. Metallkd.*, *61* (1970) 22.
14 M. Yu. Tesljuk, P. I. Kripyakevich and D. P. Frankevich, *Sov. Phys. — Crystallogr.*, *9* (1965) 469.
15 P. Eckerlin and H. Kandler, *Landolt-Börnstein, New Series*, Group III, Vol. 6, Springer, Berlin, 1971.
16 F. E. Wang and J. R. Holden, *Trans. Metall. Soc. AIME*, *233* (1965) 731.
17 J. H. Wernick and S. Geller, *Trans. Metall. Soc. AIME*, *218* (1960) 866.
18 N. C. Baenziger and J. L. Moriarty, Jr., *Acta Crystallogr.*, *14* (1961) 948.
19 H. R. Kirchmayr, *Z. Kristallogr.*, *124* (1967) 152.
20 J. H. Wernick and S. E. Haszko, *J. Phys. Chem. Solids*, *18* (1961) 207.
21 P. I. Kripyakevich and D. P. Frankevich, *Sov. Phys. — Crystallogr.*, *10* (1966) 468.
22 F. E. Wang and J. V. Gilfrich, *Acta Crystallogr.*, *21* (1966) 476.
23 P. I. Kripyakevich, D. P. Frankevich and Yu. V. Voroshilov, *Poroshk. Metall.*, *11* (1965) 55; *Chem. Abstracts*, *64* (1966) 6241f.
24 H. Oesterreicher, *J. Less-Common Met.*, *23* (1971) 7.
25 C. Nair and H. Oesterreicher, *J. Less-Common Met.*, *24* (1971) 237.
26 G. R. Pulliam and E. S. Fitzsimmons, *Rep. ISC-659*, 1955 (U.S. Atomic Energy Commission), cited in D. T. Livery and P. Murray, The stability of refractory materials". In J. O'M. Bokris, J. L. White and J. D. Mackenzie (eds.), *Physicochemical Measurements at High Temperatures*, Butterworths, London, 1959, Chapter 4, p. 96.
27 E. Parthé and B. Chabot, Crystal structures and crystal chemistry of ternary rare earth–transition metal borides, silicides and homologues. In K. A. Gschneidner, Jr., and L. Eyring (eds.), *Handbook on the Physics and Chemistry of Rare Earths*, Vol. 6, North-Holland, Amsterdam, 1984.
28 N. L. Eatough and H. T. Hall, *Inorg. Chem.*, *11* (1972) 2608.
29 A. V. Tsvyashchenko and S. V. Popova, *J. Less-Common Met.*, *90* (1983) 211.
30 J. Rhyne, K. Hardman, S. Malik and W. Wallace, in G. J. McCarthy, J. J. Rhyne and H. B. Silber (eds.), *Rare Earths in Modern Science and Technology*, Vol. 3, Plenum, New York, 1982, p. 391.
31 P. C. M. Gubbens, A. M. Van der Kraan and K. H. J. Buschow, *J. Magn. Magn. Mater.*, *30* (1983) 383.
32 C. E. Crowder and W. J. James, *J. Less-Common Met.*, *95* (1983) 1.